Solar Energy 301 (2025) 113891

Contents lists available at ScienceDirect

Solar Energy

journal homepage: www.elsevier.com/locate/solener

Comprehensive analysis and insights into the relationship between temperature coefficients, PV failures, and investigating their correlation with other PV parameters

N. Belhaouas [a,*], H. Hafdaoui [a], J.M. Nunzi [b], S. Khatir [c], D. Ernst [d], F. Mehareb [a], N. Madjoudj [a], H. Assem [a], D. Saheb-Koussa [a]

[a] Centre de Développement des Energies Renouvelables, CDER, B.P. 62, Route de l'observatoire, Bouzaréah, 16340, Alger, Algeria
[b] Department of Physics, Engineering Physics & Astronomy Queen's University 64 Bader Ln, Kingston, Ontario, K7L 3N6, Canada
[c] Center for Engineering Application and Technology Solutions, Ho Chi Minh City Open University, Ho Chi Minh, Viet Nam
[d] Department of Computer Science and Electrical Engineering, ULiége, Liége, Belgium

ARTICLE INFO

Keywords:
Photovoltaic (PV) energy
PV modules performance
PV degradation
Failure detection
Temperature coefficients
IEC 61215

ABSTRACT

Ensuring long-term performance and reliability of photovoltaic (PV) modules is essential for minimizing maintenance costs and supporting large-scale solar deployment — particularly in regions like Algeria, where solar energy plays a key role in national energy transition strategies. Among the key performance indicators, temperature coefficients (TCs) offer valuable insights into how PV parameters respond to temperature changes. While TCs are routinely included in manufacturer datasheets, their potential use as diagnostic tools for identifying and understanding failure mechanisms remains insufficiently explored. This work presents a comprehensive analysis of the relationship between temperature coefficients and PV module degradation, with a focus on enhancing failure detection and performance evaluation. Five PV module types, exposed to real outdoor conditions under Mediterranean climatic conditions for periods ranging from 4 to 30 years, were investigated through a series of inspections conducted in accordance with IEC 61215 and related standards. These included visual and thermal inspections, (I–V) curve measurements, electrical parameter assessments, and internal resistance evaluations. Furthermore, new differential ratios are introduced to improve comparative analysis. The analysis emphasizes three key datasheet-provided TCs: maximum power ($TC_{P_{max}}$), open-circuit voltage ($TC_{V_{oc}}$), and short-circuit current ($TC_{I_{sc}}$), while also drawing insights into derived coefficients such as maximum voltage ($TC_{V_{mpp}}$), maximum current ($TC_{I_{mpp}}$), and fill factor (TC_{FF}). Results reveal that both optical (e.g., discoloration, delamination) and non-optical (e.g., hot spots, corrosion) failures influence TC behavior. In particular, $TC_{P_{max}}$ shows strong sensitivity to failure occurrence and distribution, while $TC_{V_{oc}}$ closely correlates with observed thermal distribution. Although $TC_{I_{sc}}$ shows higher measurement uncertainty under outdoor conditions, its degradation appears linked to optical failure. The findings suggest that TCs, beyond their conventional use, can serve as practical indicators of specific degradation mechanisms, offering a complementary or alternative approach to existing failure detection or diagnostic techniques. The paper also recommends that manufacturers expand datasheet specifications to include additional temperature coefficients (TCs) to enhance PV module failure detection and enable more accurate performance comparisons. The paper also recommends that manufacturers expand datasheet specifications to include additional TCs for enhanced PV module failure detection and TCs values comparison. Future work will aim to refine this methodology through expanded datasets and more precise uncertainty quantification under varying environmental conditions.

1. Introduction

Photovoltaic (PV) energy is one of the most important renewable energy sources that plays a crucial role in the transition to sustainable energy in many countries, including Algeria [1,2]. Algeria's energy transition program relies significantly on this energy source [3–5]. However, the success of such a program is influenced by multiple challenges and constraints [6,7]. One major issue is the degradation and failure of PV modules, which result from material deterioration,

* Corresponding author.
E-mail address: n.belhaouas@cder.dz (N. Belhaouas).

https://doi.org/10.1016/j.solener.2025.113891
Received 26 May 2025; Received in revised form 16 July 2025; Accepted 15 August 2025
Available online 27 August 2025

climatic conditions, and operational factors [8–10]. These issues can shorten the lifespan of PV modules, potentially affecting the economic viability and long-term profitability of PV installations, thereby posing a risk to the overall effectiveness of the energy transition strategy [11, 12].

PV modules are susceptible to various failure mechanisms throughout their lifespan, some of which can significantly impact their performance, potentially leading to premature failure before reaching the manufacturer's guaranteed lifetime [13,14]. However, relying only on qualification standards such as IEC 61215 is insufficient to ensure high performance over 25 years of outdoor operation under diverse climatic and working conditions, as these standards do not fully prevent failure occurrences [15–17]. Therefore, it is crucial to apply advanced techniques and methodologies for continuous performance assessment throughout the module's lifetime [18–20]. Early-stage PV module failures such as delamination, localized heating (hot spots), and initial encapsulant discoloration often precede severe performance losses. These failures can be detected through continuous monitoring and inspections using electrical characteristic curve tracing, visual, and infrared failures thermography along with other inspections. Implementing such techniques enables early intervention and can extend the operational lifespan of modules before catastrophic or irreversible degradation occurs [21–24]. Nevertheless, these methods still face limitations in accurately identifying failures, particularly in terms of occurrence, severity, and distribution, due to the complex nature of failure mechanisms influenced by multiple factors [25]. A comprehensive understanding of PV performance and failure mechanisms is essential for improving failure detection methods [26,27]. Therefore, developing an advanced approach that integrates the strengths of existing diagnostic techniques while establishing correlations between them can significantly enhance the accuracy of failure identification and help overcome their limitations.

Recent research has extensively assessed PV performance and degradation across various climates, providing valuable data for correlating performance loss with inspection outcomes [28,29]. These efforts have advanced different diagnostic tools, such as visual inspection [30], thermographic imaging [31], (I-V) curve analysis [32,33], electrical parameter monitoring [34], and resistance modeling [35]. Nonetheless, many of these tools fall short in detecting early-stage or compound failures without integration or enhancement. However, recent studies have further explored the temporal evolution of temperature coefficients and their connection to long-term degradation trends. For example, Perin Gasparin et al. [36] analyzed how TCs change with aging across different climates and PV technologies, emphasizing their value in lifetime performance prediction. Furthermore, Rahaman et al. [37] demonstrated how thermal imaging data can be used in conjunction with electrical parameters to identify early-stage degradation, highlighting the benefit of integrating thermographic behavior into fault diagnostics. One promising approach to addressing this issue is by considering the impact of PV module temperature on performance and degradation. In which, temperature plays a dual role in PV module behavior: it causes an immediate reduction in power output-particularly, and it also accelerates long-term degradation processes [38]. Elevated operating temperatures have been associated with faster rates of encapsulant browning, solder joint fatigue, corrosion, and delamination, all of which contribute to electrical parameter shifts and performance decline [39]. As a result, PV module temperature illustrated by the temperature coefficients (TCs) not only serve as essential indicators of efficiency loss but may also function as early diagnostic markers of material and electrical degradation. This relationship, though significant, remains underutilized in failure analysis. Despite the significance of this factor, few studies have examined the detailed determination of temperature coefficients. For instance, Perin Gasparin et al. [36] proposed a method to extract TCs from outdoor data, while Senturk [40] investigated TC behavior under varying irradiance levels. However, these works primarily focused on characterization and model fitting rather than diagnostic applications. Notably, Wang et al. [41] explored the potential of TC deviation as an early indicator of failure, yet did not establish a consistent link between specific degradation modes and individual TC shifts. Therefore, despite the recognized value of temperature coefficients in performance modeling, their use as diagnostic indicators for specific PV failure modes has received limited attention. Most studies focus on TC trends without correlating them to concrete visual, thermal, or electrical degradation signatures. This study addresses this gap by exploring how changes in key temperature coefficients can reflect the presence, severity, and type of failure mechanisms observed in long-term outdoor-exposed PV modules. The novelty of this work lies in integrating temperature coefficient analysis with a suite of diagnostic tools-including thermographic imaging, (I–V)/(P–V) curves measurements, and internal resistance determination-to develop a more holistic and early-stage failure detection framework.

This paper focuses on analyzing key temperature coefficients-including short-circuit current ($TC_{I_{sc}}$), open-circuit voltage ($TC_{V_{oc}}$), maximum power ($TC_{P_{max}}$), and fill factor (TC_{FF}) - to evaluate their sensitivity to observed failures. These are linked via the expression:

$$TC_{P_{max}} = TC_{I_{sc}} + TC_{V_{oc}} + TC_{FF}$$

[42], with (TC_{FF}) further related to ($TC_{I_{mpp}}$) and ($TC_{V_{mpp}}$). In this work, the determination of these temperature coefficients has been presented and briefly discussed. However, the analysis primarily focuses on the temperature coefficients provided in the datasheet. To achieve this, five PV module types with different outdoor exposure durations have been selected, considering only the best- and worst-performing module samples. These modules have undergone a series of inspections, including failure imaging (visual and thermal), electrical parameter assessments, temperature coefficient analysis, and internal resistance determination. This paper not only enhances the understanding of temperature coefficient behavior but also investigates potential correlations between temperature coefficients and failure occurrence, severity, and distribution, alongside other inspection results. The findings obtained may serve as either an alternative or a complementary technique for failure detection, offering a novel approach to improving existing diagnostic methods in the literature.

2. Methodology

2.1. Description of PV module samples and types

This work has examined five PV installations, each subjected to different durations of outdoor exposure — specifically 30, 17, 11, 07, and 04 years-under Mediterranean climate conditions. The selected modules represent two technologies: monocrystalline silicon (m-Si) and polycrystalline silicon (p-Si). Electrical inspections have been conducted on all PV modules within these installations. For each PV module type (i.e., from separate installations), the best- and worst-performing samples have been selected based on their power output measured under conditions approximating Standard Test Conditions (STC: 1000 W/m^2, 25 °C). This comparative selection aims to assess the influence of degradation severity on both electrical performance and temperature coefficient behavior. The key PV parameters corresponding to each module type are summarized in Table 1.

2.2. Description of PV module inspections

2.2.1. Imaging failures inspections

This inspection has been conducted using two complementary methods in accordance with IEC 61215-2-4:2016 recommendations: visual failure inspection and thermal failure inspection [43,44]. The visual inspection has focused on identifying and localizing defects such as discoloration, delamination, cracking, broken finger, or corrosion failures through direct observation under uniform daylight conditions. The thermal inspection has been carried out using a calibrated FLIR infrared

Table 1
The PV parameters of different PV module types.

PV modules	A	B	C	D	E
PV Technology	m-Si	m-Si	m-Si	p-Si	p-Si
Time in field (years)	30	07	11	17	04
P_{max} (W)	43	50	75	150	255
V_{oc} (V)	21.7	21.6	21.6	43.2	37.4
I_{sc} (A)	2.7	3.2	4.67	4.8	9
I_{max} (A)	2.49	2.9	4.34	4.3	8.43
V_{max} (V)	17.3	17.2	17.3	35	30.2
FF (%)	73.39	72.33	74.35	72.33	75.75
R_{oc} (Ω)	0.65	0.55	0.35	0.58	0.31
R_{sh} (Ω)	262.28	133.69	206.18	137.38	366.47
$TC_{I_{sc}}$ (%/°C)	0.074	0.045	0.06	0.029	0.065
$TC_{V_{oc}}$ (%/°C)	−0.41	−0.36	−0.36	−0.34	−0.34
$TC_{P_{max}}$ (%/°C)	−0.48	−0.43	−0,48	−0.46	−0.43
Area (m^2)	0.37	0.46	0.66	1.28	1.6

camera (Model T640), to detect temperature failures associated with internal failures.

Thermal images have been captured under stable outdoor irradiance conditions above 700 W/m^2, typically between 11:00 and 14:00, to ensure sufficient thermal contrast. The camera was positioned perpendicularly (at a 90° angle) to the PV module surface, at a fixed distance of 1.5 m, with an emissivity setting of 0.95-appropriate for common PV encapsulant surfaces. Efforts have been made to minimize environmental reflections during image acquisition to improve thermal accuracy [43,45].

Thermal anomalies have been classified into three severity categories(minor, under observation, and critical) based on the measured temperature difference (∂_{Temp}) between the hottest cell region and the coldest cell in the module. The classification thresholds are as follows:

- $\partial_{Temp} < 10\,°C$ (minor),
- $10\,°C \leq \partial_{Temp} < 30\,°C$ (under observation),
- $\partial_{Temp} \geq 30\,°C$ (critical, typically indicating a hot spot).

These classifications reflect the potential severity of thermal-related degradation and are summarized for each module type in Table 2.

Different failure mechanisms have exhibited distinct thermal signatures across the investigated PV modules. Optical failures such as delamination or discoloration have generally led to broad, thermal inhomogeneity distribution heating patterns across cells. In contrast, non-optical failures like solder joint corrosion, interconnect breakage, or hot spots have produced localized high-temperature zones aligned with cell edges or interconnect lines. These observed patterns have helped support diagnostic classification and correlation with electrical parameter deviations, particularly in relation to the temperature coefficients.

2.2.2. Electrical parameters inspections

This inspection involves tracing the (I–V) and (P–V) characteristic curves under conditions approximating STC. Based on the plotted curves, key PV parameters have been determined, including I_{sc}, V_{oc}, I_{mpp}, V_{mpp}, P_{max}, and FF. The outdoor measurement tests have been carried out using a dedicated experimental setup developed for this purpose, as depicted in Fig. 1. In which, the setup includes a sun-tracking structure to maintain optimal irradiance alignment, a PV characteristics curve tracer, and a data acquisition and monitoring system developed in LabVIEW. This system incorporates instruments such as a Keysight N3301A electronic load, a Keysight 34972A data logger, Si-01TC-T thermocouples, and additional environmental sensors for irradiance, ambient temperature measurements and module surface temperature [44]. All measurements have been conducted in accordance with the IEC 61215-2:2016 standard, ensuring traceability and accuracy. in this regards, to ensure accurate electrical measurements under conditions approximating STC, a standardized preconditioning and cooling protocol has been applied. Each PV module is first shaded and allowed to cool naturally until its surface temperature approaches ambient levels typically around 15 °C. After stabilization, the module is rapidly exposed to full sunlight when the irradiance reaches 1000 W/m^2 (within a tolerance of ±2%) and the module temperature reaches 25 °C (also within a tolerance of ±2%). The (I–V) and (P–V) curves are then recorded immediately within a few seconds to minimize the effects of temperature rise. Multiple trials are repeated within a narrow irradiance and temperature window, and only the most stable measurements are retained for analysis, see Fig. 2. This approach ensures that transient heating does not bias the recorded performance metrics [43]. Furthermore, the extracted data from these curves have been used not only to calculate essential performance parameters but also to identify abnormal behaviors and failure signatures. These results serve as input for subsequent temperature coefficient and internal resistance determination. It is worth noting that the experimental setup and outdoor measurement procedures have been conducted in accordance with IEC 61215-2:2016, IEC 60904-1:2006, and IEC 60891:2009 to ensure high accuracy and reliability in (I–V) curve acquisition and temperature coefficient determination. These standards guided sensor placement, data acquisition protocols, and environmental monitoring. All equipment used was brand new, properly calibrated, and certified at the time of testing. To minimize uncertainty, measurements were repeated within narrow irradiance and temperature windows. While degradation rates are calculated by comparing measured data to nameplate values (typically toleranced within ±3%), minor deviations may still occur due to instrument precision limits and inherent datasheet variability. Note: uncertainty values will be detailed in future work.

2.2.3. Temperature coefficient determination

The determination of temperature coefficients involves identifying three primary coefficients ($TC_{I_{sc}}$, $TC_{V_{oc}}$, and $TC_{P_{max}}$) based on the values provided in the datasheets of the selected PV module samples. The objective is to compare the experimentally obtained coefficients with those provided by the manufacturer.

These temperature coefficients have been determined in accordance with IEC 61215-2 by tracing the characteristic curves at 1000 W/m^2 under varying temperature conditions. The procedure ensures that the PV module temperature increases by at least 30 °C, with I–V curve measurements taken at approximately every 2 °C increment, repeat the steps outlined in the flowchart shown in Fig. 2, and a linear regression method has been applied to extract the temperature coefficients from the resulting data. While this approach is based on controlled outdoor measurements (see Fig. 1), it is important to note that other methods exist for estimating temperature coefficients using long-term monitored data and statistical modeling, as described by Paudyal and Imenes [42]. However, in this work, we rely on the direct I–V curve tracing method, which complies with standard procedures and provides reliable estimates of the targeted coefficients for diagnostic analysis. For more details on our performed experimental and measurement setup, as well as the test procedure description, refer to our previous work [43]. However, $TC_{I_{sc}}$ has been excluded from this work due to challenges encountered during outdoor measurement tests [46]. In which, each (I–V) scanning process has required approximately 1–2 min per module and has provided reliable measurements of the key PV parameters. In contrast, the complete procedure for determining temperature coefficients has taken about 20 min per PV module sample, ensuring adequate thermal variation for accurate coefficient extraction. During this period, slight variations in irradiance have introduced significant linear deviations exceeding permissible tolerance values, as defined by IEC 60904-10. These deviations have mainly compromised the accuracy and reliability of the calculated temperature coefficient for current, while other parameters have remained within acceptable limits. As a consequence, $TC_{I_{sc}}$ has been omitted to ensure the integrity and validity of the findings. On the other hand, the same measurement

(a) (b)

Fig. 1. Characteristics of the deployed PV module sample: (a). outdoor mobile structure for solar tracking. (b). Software and hardware for PV curve tracing (I–V and P–V).

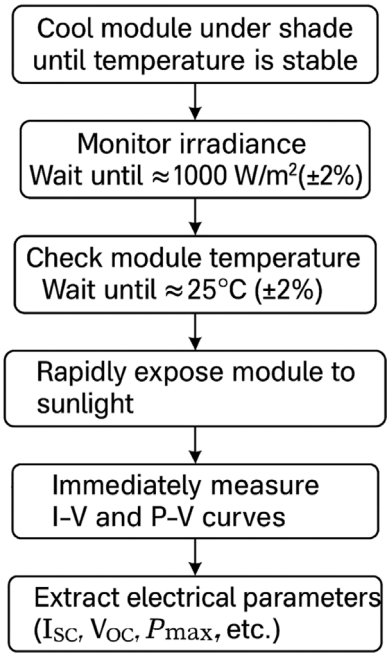

Fig. 2. Flowchart of the performed outdoor electrical measurement procedure.

setup and procedures could be applied to determine additional temperature coefficients, such as $TC_{I_{mpp}}$, $TC_{V_{mpp}}$, and TC_{FF}, which correspond to parameters like V_{max}, I_{max}, and FF. Note, other methods can also determine these three coefficient values in real-time, except for $TC_{V_{oc}}$ and $TC_{I_{sc}}$, as detailed in the Ref. [47]. However, these coefficients have not been covered in this work, as the focus remains on those explicitly provided in the datasheets.

2.2.4. Internal resistance determination

The determination of internal resistance values, specifically the series resistance (R_{oc}) and shunt resistance (R_{sh}), has been conducted using measured PV parameters (I_{sc}, V_{oc}, and P_{max}) for the deployed PV module samples [48]. Furthermore, this method has been applied to compute reference internal resistance values for each PV module type based on datasheet specifications, as presented in Table 1. In this regards, the Newton–Raphson method, an iterative algorithm, has been applied [49]. To ensure optimal convergence and accurate determination of both internal resistance values, the initial inputs for the algorithm have been carefully chosen.

2.2.5. PV parameter rate calculations

Several parameter ratios have been employed in this work to quantify the significance of various PV performance parameters. Among these, the degradation rate (DR) is a commonly used metric to describe the degradation of electrical parameters (see Eq. (1)). Furthermore, the yearly degradation rate (YDR), derived from the degradation rate (DR), has been introduced (see Eq. (2)) by incorporating the number of years of service into Eq. (1).

$$DR = \frac{((Data\_Initial) - (Data\_Final))}{(Data\_Initial)} \times 100 \quad (1)$$

$$YDR = \frac{(DR)}{\Delta T} \quad (2)$$

New differential rate (Δ) has also been employed in this work to provide a clearer interpretation when addressing these PV parameters or others, by considering specific reference values, see Eq. (3). The initial reference values used for calculating the differential rates (Δ) of the electrical parameters (P_{max}, I_{sc}, and V_{oc}) have been derived based on the yearly degradation rates expected under the local climatic conditions, corresponding to 0.8%, 0.5%, and 0.07%, respectively. Meanwhile, the initial reference values for internal resistances and temperature coefficients have been computed and obtained from the datasheet, respectively, as given in Table 1.

$$\Delta = \frac{((Data\_Final) - (Data\_reference))}{(Data\_reference)} \times 100 \quad (3)$$

3. Results, comparison, and correlation analysis

The (I–V) and (P–V) characteristic curves of the best- and worst-performing PV modules from each type (A, B, C, D, and E) are presented in Fig. 4.

Table 2 summarizes the corresponding electrical data, including yearly degradation rates, differential variations in key performance parameters (I_{sc}, V_{oc}, P_{max}, FF), internal resistances (R_{oc}, R_{sh}), and temperature coefficients ($TC_{V_{oc}}$, $TC_{P_{max}}$). Also included is the thermal variation index (∂_{Temp}), representing the highest temperature difference among cells within the same module, as identified through thermal inspection. Furthermore, Fig. 5 illustrates various failure types observed during visual inspections. In this figure, the initial letter corresponds to the PV module type, the subscript denotes the failure count in

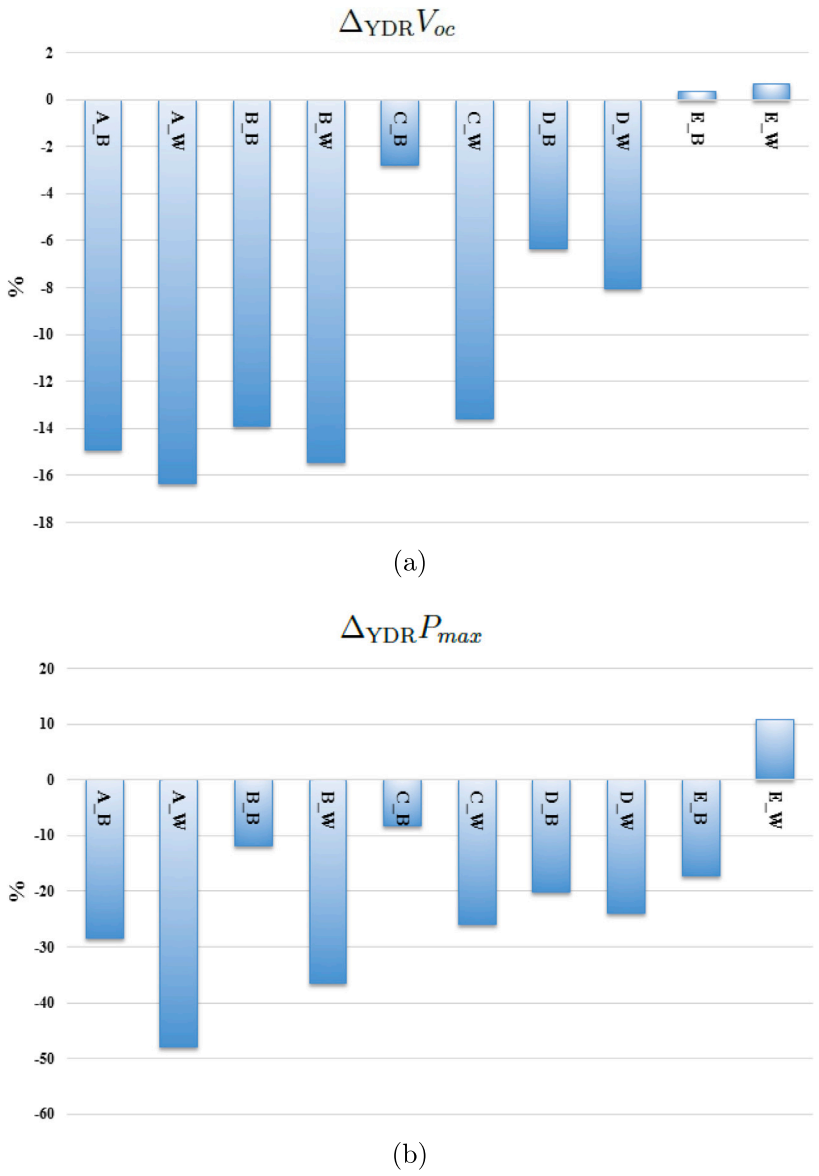

Fig. 3. Degradation rates of temperature coefficients for all samples (best- and worst-performing) across different PV module types: (a). $\Delta_{YDR}V_{oc}$. (b). $\Delta_{YDR}P_{max}$.

the same module, and the letters (B) and (W) indicate the best- and worst-performing modules, respectively.

To enhance clarity and visualization, a graphical comparison between the manufacturer-specified and experimentally estimated temperature coefficients (illustrated through the degradation rate of both $TC_{V_{oc}}$ and $TC_{P_{max}}$) has been included, as shown in Fig. 3. This comparison highlights the extent of deviation from nominal values and provides visual insight into how different failure types and their severity, and deviation between the best and worst performing PV samples influence temperature coefficients.

All results have been analyzed in detail, with special attention given to identifying correlations between observed failures, electrical performance, and temperature coefficient degradation. These relationships are discussed and outlined below:

3.1. Results discussion

3.1.1. Type A

The Type A PV modules have been exhibiting significant discoloration (browning) and finger disconnection failures, as observed through visual inspection. Due to the high severity and occurrence of discoloration, this failure has been considered the dominant failure. The best-performing PV sample has shown these failures, with thermal inspection indicating notable inhomogeneity in thermal distribution, with temperature difference (∂_{Temp}) of up to 20 °C, though no hot spots have been detected, as outlined in Table 2. Electrical inspection has revealed a slight increase in the yearly degradation rate under local climatic conditions, with a $\Delta_{YDR}P_{max}$ of 38.46%, and corresponding increases in $\Delta_{YDR}I_{sc}$ and $\Delta_{YDR}V_{oc}$ by 6.17% and 95.30%, respectively; where the fill factor (FF) exhibited a significant decline of 49%. Furthermore, internal resistance measurements have shown a 169.23% increase in ΔR_{oc} and a slight decrease of −64% in ΔR_{sh}. In addition, temperature coefficients for $\Delta_{TC_{V_{oc}}}$ and $\Delta_{TC_{P_{max}}}$ have decreased by −14.92% and −28.53%, respectively. On the other hand, the worst-performing PV sample has exhibited increased severity of dominant failure, particularly discoloration, progressing from light to dark browning, which, it has been an increased in both the area and occurrence number as well as for broken interconnections of the PV fingers. Meanwhile, thermal inspection has revealed a medium level of inhomogeneity in the module's thermal distribution, with a temperature difference (∂_{Temp}) of less than 30 °C, indicating no hot spots. The electrical inspection of this sample has shown increases across all degradation PV parameters,

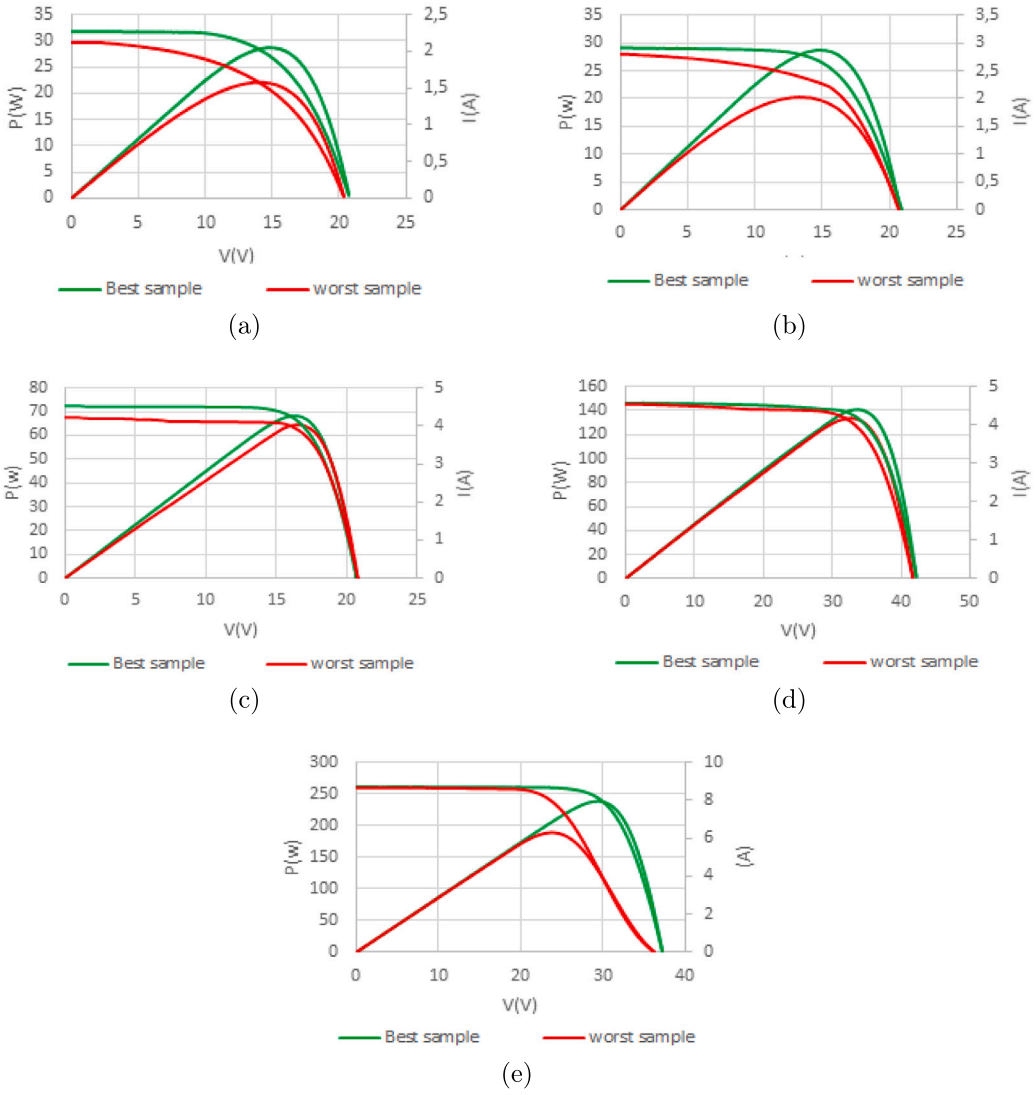

Fig. 4. Measured (I–V), and (P–V) characteristic curves for the both best and worst performing PV module sample of all five module types (A:E) under STC conditions.

Table 2
Summary of PV parameter degradation rates for all samples across different PV module types.

PV types	A		B		C		D		E	
PV samples	A_B	A_W	B_B	B_W	C_B	C_W	D_B	D_W	E_B	E_W
∂_{Temp} (°C)	20	30	10	20	20	30	20	25	30	100
FF (%)	49	37.7	57.29	49.92	67.62	63.9	67.51	64.41	70.92	56.15
$YDR_{I_{sc}}$	0.53	0.66	0.60	0.83	0.27	0.87	0.27	0.32	0.80	0.91
$YDR_{V_{oc}}$	0.13	0.19	0.21	0.28	0.34	0.38	0.13	0.2	0.12	0.90
$YDR_{P_{max}}$	1.10	1.62	1.36	2.09	0.82	1.27	0.35	0.64	1.59	6.46
$\Delta_{YDR} I_{sc}$	6.17	33.33	20.83	66.66	−45.06	74.79	−46	−36	61.11	83.33
$\Delta_{YDR} V_{oc}$	95.30	183.08	213.05	305.64	392.24	452.12	85.71	185.71	71.88	1198.70
$\Delta_{YDR} P_{max}$	38.46	102.61	70.83	161.66	2.75	59.57	−56.25	−20	99.26	708.70
ΔR_{oc}	169.23	250.76	105.45	127.27	14.28	11.42	29.31	51.72	248.38	1025.80
ΔR_{sh}	−64.77	−85.39	−4.18	−41.62	−4.59	−27.31	−1.46	−7.88	−56.77	−94.61
$\Delta_{TC_{I_{sc}}}$	–	–	–	–	–	–	–	–	–	–
$\Delta_{TC_{V_{oc}}}$	−14.92	−16.37	−13.92	−15.44	−2.77	−13.61	−6.34	−8.07	0.34	0.66
$\Delta_{TC_{P_{max}}}$	−28.53	−47.81	−11.86	−36.44	−8.33	−25.87	−20.12	−23.91	−17.20	10.91

with $\Delta_{YDR} I_{sc}$, $\Delta_{YDR} V_{oc}$, and $\Delta_{YDR} P_{max}$ increasing by 33.33%, 183.08%, and 102.61%, respectively; and FF has noticeably decreased by 37.7%. Internal resistances have also shown significant variation, with ΔR_{oc} increasing by 250.76%, while ΔR_{sh} has decreased by −85.69%. Regarding temperature coefficients, there has been a slight change in $\Delta_{TC_{V_{oc}}}$, but a significant reduction in $\Delta_{TC_{P_{max}}}$, decreasing by −16.37% and −47.81%, respectively.

3.1.2. Type B

Visual failure inspections have been revealing that Type B PV modules suffer from delamination along bus bars across all PV cells,

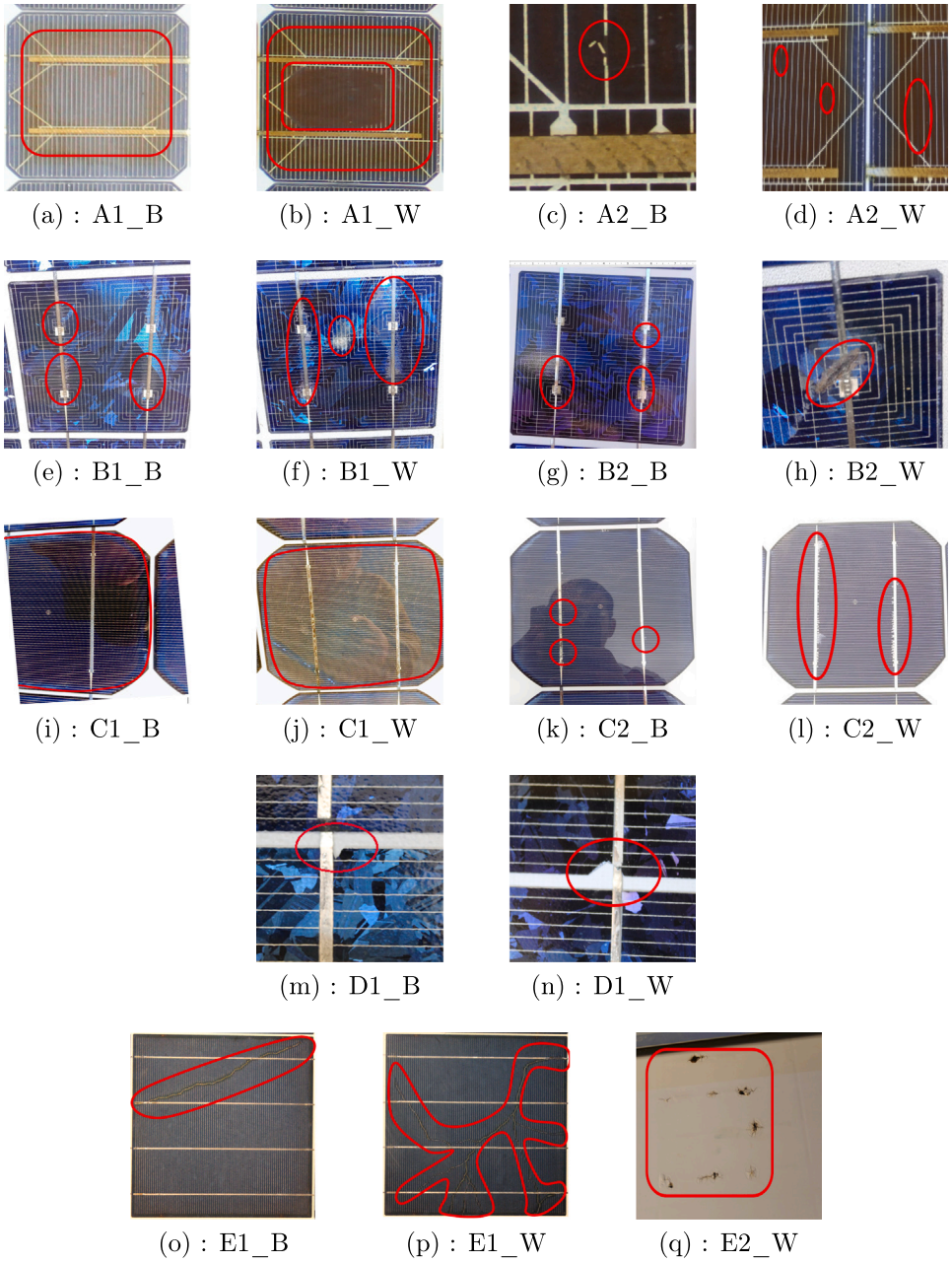

Fig. 5. Visual failures images of some PV module samples of different PV types (A-E): Type A: (A1). Discoloration: (A1_B). low severity, (A1_W). high severity. (A2). Broken PV fingers: (A2_B). few ones, (A2_BW). several ones. Type B: (B1). Delamination: (B1_B). small area, (B1_W). large area. (B2). Corrosion: (B2_B). low severity, (B2_W). high severity. Type C: (C1). Discoloration: (C1_B). low severity, (C1_W). high severity, (C2): Delamination: (C2_B). small area, (C2_W). large area. Type D: (D1). PV cell fragmentation: (D1_B). small area, (D1_W). large area. Type E: (E1). Micro cracking (snail trail): (E1_B). small area, (E1_W). large area. (E2): Hot spot (E1_W). burn marks.

with additional corrosion observed on certain bus bars. Due to its high occurrence relative to other failure types, delamination has been classified as the dominant failure within the optical failure category. The best-performing PV module sample has primarily exhibited delamination, with thermal inspections indicating a low level of thermal inhomogeneity, where the maximum temperature difference (∂_{Temp}) between PV cells has not exceeded 10 °C, and no hotspots have been observed. Electrical inspection of this selected PV sample has shown that differential yearly degradation rates (Δ_{YDR}) for the PV electrical parameters (I_{sc}, V_{oc}, and P_{max}) have significantly increased, with $\Delta_{\mathrm{YDR}} I_{sc}$, $\Delta_{\mathrm{YDR}} P_{max}$, and especially $\Delta_{\mathrm{YDR}} V_{oc}$ exceeding expected rates by over 20%, 70%, and 200%, respectively, see Table 2. Moreover, FF has been decreased by 57.29%. For internal resistances, the differential resistance rate ΔR_{oc} of the best-performing module has increased by 105.4% compared to its initial datasheet value, while the R_{sh} has shown a slight decrease of 4%. Furthermore, temperature coefficients $\Delta_{TC_{V_{\mathrm{oc}}}}$ and $\Delta_{TC_{P_{\mathrm{max}}}}$ have decreased relative to datasheet values by −13.92% and −11.86%, respectively. In contrast, the worst-performing PV module has exhibited an increase in the severity of delamination, especially in terms of affected area, although corrosion-related failures have shown no substantial change. Thermal inhomogeneity has also increased, with a ∂_{Temp} of up to 20 °C, though no hotspots have been detected. This PV module further demonstrated high Δ_{YDR} values for the PV parameters $\Delta_{\mathrm{YDR}} I_{sc}$, $\Delta_{\mathrm{YDR}} V_{oc}$, and $\Delta_{\mathrm{YDR}} P_{max}$, surpassing expected

rates by approximately 66.6%, 305.64%, and 161.66%, respectively. In addition, the FF has shown a substantial decrease of 49.92%. Internal resistance measurements for this sample showed a substantial increase in ΔR_{oc} by 127.2%, while ΔR_{sh} decreased by about 41% from its initial value. Moreover, the temperature coefficients $\Delta_{TC_{P_{\max}}}$ and $\Delta_{TC_{V_{\mathrm{oc}}}}$ decreased by -36% and −15.44%, respectively.

3.1.3. Type C

Type C PV modules exhibit several low-severity failures, including central yellowing, and delamination [43], as observed during visual inspection. These failures, all classified as optical failures, show almost similar severity and occurrence. As a consequence, discoloration and delamination have been considered dominant failure based on their cumulative impact. The best-performing PV module also exhibits these failures, and shows low inhomogeneity in thermal distribution, with temperature variations (∂_{Temp}) between cells not exceeding 20 °C, mostly falling within the minor severity category. Notably, two PV cells display significant temperature variation, although no hot spots have been observed. Electrical inspection reveals that this tested PV module demonstrates high electrical performance, particularly regarding the yearly degradation rates (YDR) of parameters such as (P_{max}, and I_{sc}). However, the V_{oc} shows a significantly higher degradation rate than anticipated for the given climate conditions, as indicated by the differential yearly degradation rate (Δ_{YDR}). Specifically, the Δ_{YDR} for I_{sc} and P_{max} indicates high performance in this PV sample, with values of −45% and +2.75%, respectively, while the $\Delta_{\mathrm{YDR}} V_{oc}$ exhibits a substantially elevated rate, exceeding the expected rate by 392.24%; and the FF has exhibited a moderate decrease of 67.62%. In terms of internal resistances, the differential rate for R_{oc} (ΔR_{oc}) increased by 14.28%, while the ΔR_{sh} remained relatively unchanged, showing only a slight decrease of (ΔR_{sh}, −4%), and regarding temperature coefficients, the both coefficients ($\Delta_{TC_{V_{\mathrm{oc}}}}$ and $\Delta_{TC_{P_{\max}}}$) have decreased relative to their initial value rate −2.7% and −8.3%, respectively. On the other hand, the worst performed PV module suffer from the dominate failure with a slightly high occurrence, these failures include noticeable corrosion along the bus bars and soldering points. Thermal inspection reveals that this PV sample exhibits a high temperature variation across its cells (∂_{Temp}), reaching up to 30 °C. Meanwhile, electrical inspection reveals a noticeable decline in performance, with yearly degradation rates ($\Delta_Y DR$) for I_{sc} and P_{max} showing decreases of 74.79% and 59.57%, respectively. Although the V_{oc} shows slight increased, its degradation rate remains high, with $\Delta_{\mathrm{YDR}} V_{oc}$ of 452%. While, the FF has decreased by 63.9%. In terms of internal resistance, the ΔR_{oc} has increased by 11.42%, while the ΔR_{sh} has significantly decreased by −27.31%. Regarding the temperature coefficients, both $\Delta_{TC_{P_{\max}}}$ and $\Delta_{TC_{V_{\mathrm{oc}}}}$ show significant decreases of −13.61% and −25.87%, respectively.

3.1.4. Type D

Upon visual inspection, it has been revealed that the Type D PV module predominantly suffers from PV cell fragmentation, with only minimal discoloration present. The best-performing PV sample has been demonstrating a high occurrence of cell fragmentation while maintaining very low discoloration across all PV cells in the sample. Thermal inspection has further indicated that this sample exhibits low inhomogeneity in temperature distribution, remaining below 20 °C. Electrical inspection has shown high performance in terms of I_{sc} and P_{max}, with differential yearly degradation rates with -46% and −56.2%, respectively. However, V_{oc} performance has been lower, as reflected by a relatively high degradation rate, with an $\Delta_{\mathrm{YDR}} V_{oc}$ of 85.71%. Furthermore, the FF has shown a relatively low decrease 67.51%. The internal resistances have exhibited varied behavior: R_{oc} has shown a noticeable increase of 29%, while R_{sh} has been relatively low, decreasing only slightly by −1.46%. Furthermore, the temperature coefficients reveal that $TC_{V_{oc}}$ has decreased by −6.3%, whereas $TC_{P_{max}}$ has decreased significantly by −20%. In contrast, the worst-performing PV sample has also been exhibiting discoloration, with a lower occurrence of PV cell fragments; however, these fragments cover a larger area compared to those in the best-performing module. Thermal inspection has revealed slight inhomogeneity in its temperature distribution, with variations remaining below 25 °C. Despite these issues, the worst-performing sample has been maintaining high performance for I_{sc} and P_{max}, with differential yearly degradation rates (Δ_{YDR}) of −36% and −20%, respectively. However, V_{oc} has shown a significant increase, with an Δ_{YDR} of 185.7%; and The FF has experienced a relatively low decrease of 64.41%. In addition, the internal resistances have exhibited distinct trends: R_{oc} has significantly increased by 51.7%, while R_{sh} has decreased slightly by −7.8%. The temperature coefficient $TC_{V_{oc}}$ has shown a low decreased of −8%, while $TC_{P_{max}}$ has decreased more noticeably by −23.9%.

3.1.5. Type E

Type E PV modules predominantly suffer from snail trails (Microcracks) accompanied by burn marks along the trails, making this the dominate observed failure. The best-performing PV sample exhibits several PV cells affected by this failure, some with hotspots on their backsheets. This PV sample exhibits high inhomogeneity, with multiple PV cells classified as critical failure and a temperature variation exceeding 30 °C. Electrical inspection indicates that the best-performing sample has a lower-than-expected performance, attributed to an increase in yearly degradation rates across all electrical parameters (I_{sc}, V_{oc}, and P_{max}), with Δ_{YDR} of 61.1%, 71.8%, and 99.2%, respectively. The FF has shown a very low decrease of 70.92%. The internal resistances R_{oc} and R_{sh} are significantly impacted, showing differential rates of 248.3% and −56.7%, respectively. And the temperature coefficients $\Delta_{TC_{V_{\mathrm{oc}}}}$ and $\Delta_{TC_{P_{\max}}}$ are also affected, particularly $TC_{P_{max}}$, with values of 0.34% and −17.20%, respectively. Besides, the worst-performing PV sample exhibits not only snail trail failure on several PV cells as the dominant failure also a hotspot in one of the affected cells, located in the corresponding backsheet area. Thermal inspection reveals significant thermal inhomogeneity, with hotspots exceeding 100 °C, which is considered to have a critical and dangers thermal impact. Electrical inspection shows that all electrical parameters have been drastically affected, particularly V_{oc} and P_{max}, with differential degradation yield ratio (Δ_{YDR}) values of 1198.7% and 708.7%, respectively, while I_{sc} is less affected, with a Δ_{YDR} of 83.3%. Besides, the FF has noticeably decreased by 56.15%. In terms of internal resistances, both R_{oc} and R_{sh} have been significantly impacted, with R_{oc} showing a significantly increase of 1025.8%, while R_{sh} has drastically decreased by −94.5%. Furthermore, both temperature coefficients ($\Delta_{TC_{V_{\mathrm{oc}}}}$ and $\Delta_{TC_{P_{\max}}}$) have noticeably increased, with values higher than expected at 0.66% and 10.91%, respectively.

3.2. Comparison, and correlation analysis:

3.2.1. Type A

The dominant failure (discoloration) in the Type A PV module is considered an optical failure, exhibited along with broken finger interconnections failure. In which, the both of these observed failure types have increased in terms of severity and occurrence number in the worst-performing sample compared to the best-performing PV module. Meanwhile, thermal inspections have revealed that the worst-performing modules exhibit a slight increase in thermal behavior compared to the best-performing PV sample, although no hot spots have been detected in either. Therefore, the optical nature of the dominant failure primarily affects the I_{sc}, with increased severity (illustrated by the worst PV sample) leading to a further reduction in I_{sc} and a corresponding increase in the $\mathrm{YDR}_{I_{\mathrm{sc}}}$. Similarly, greater inhomogeneity in thermal distribution primarily impacts the V_{oc} and consequently leads to an increase in $\mathrm{YDR}_{V_{\mathrm{oc}}}$. Besides, the internal resistances have also been affected by these failures: R_{oc} exhibits a high rate due to broken interconnections of the PV fingers, while R_{sh} is influenced by thermal distribution inhomogeneity. In which, the variations in both resistances

(R_{oc}, R_{sh}) increase as the severity of these failures and the degree of thermal inhomogeneity increase, respectively. As a result, the FF is low, being more strongly influenced by increases in R_{oc} than by variations in R_{sh}, primarily due to the severity of broken interconnection failures and relatively low thermal inhomogeneity. Besides, The temperature coefficients ($TC_{V_{oc}}$ and $TC_{P_{max}}$) initially show noticeably high rate values. In which, the obtained results indicate that increased failure severity significantly affects $TC_{P_{max}}$, while $TC_{V_{oc}}$ remains relatively stable. This disparity in $TC_{V_{oc}}$ is likely due to variations in thermal distribution, which correspond closely to the behavior of V_{oc}, refer to the subsection of Type E PV modules, where this relationship is more clear. Meanwhile, $TC_{P_{max}}$ values exhibit considerable variation between the selected PV samples, suggesting that increased severity of optical failure may be related to changes in $TC_{I_{sc}}$, TC_{FF}, or both, which in turn further affect $TC_{P_{max}}$.

3.2.2. Type B

Type B PV modules, across all selected samples, have primarily been suffering from delamination along the busbar, identified as the dominant failure. Meanwhile, some corrosion of bus bars is observed. Besides, the thermal inhomogeneity distribution has exhibited almost the same behavior, with a $\partial_{Temp} = 10$ °C. And concerning the electrical performance, this dominant failure (delamination), classified as an optical failure, mainly impacts the I_{sc} by reducing irradiance, which lowers current production and, As a consequence, the maximum power output (P_{max}). As delamination severity increases, as seen in the worst-performing module, the degradation rate of the two electrical parameters (I_{sc} and P_{max}) have been raised notably. Nevertheless, both module samples have shown a high degradation rate of V_{oc}, with noticeable variation in their yearly degradation rates for V_{oc} ($\mathrm{YDR}_{V_{oc}}$). Which, this consistent degradation is likely attributed to differences in thermal distribution between the PV samples. Regarding internal resistance, the increase in R_{oc} has largely been attributed to corrosion of some bus bars, and the slight increase in this failure, as illustrated by the worst-performing module, has only slightly affected the R_{oc}. Similarly, the R_{sh} decreases due to inhomogeneity distribution of various failures, with greater inhomogeneity leading to a further reduction in R_{sh}. Thus, The FF is relatively low, influenced by both internal resistances; however, in this case, it is more affected by the increase in R_{oc} than in R_{sh}, due to the high severity of corrosion compared to the relatively low thermal inhomogeneity. For temperature coefficients, $\Delta_{TC_{V_{oc}}}$ exhibits a relatively low value of −11%, with minimal variation (−1.5%) between the selected PV modules, reflecting V_{oc} behavior and consistent with $\mathrm{YDR}_{V_{oc}}$. This suggests that the impact of failure may relate to uniform failure distribution, although other factors may play a role. Furthermore, $TC_{P_{max}}$ exhibits a low rate, yet a noticeable variation in this rate has been observed between the two selected samples. This variation suggests that the severity of observed failures, particularly optical ones, significantly impacts $TC_{P_{max}}$.

3.2.3. Type C

Type C PV modules have exhibited various visible failures, primarily classified under the optical failure category, which have been all classified as the dominant failure based on their impact. In which, the severity of this dominant failure has been increasing, predominantly in terms of occurrence more than affected area, with this trend more pronounced in the worst-performing modules compared to the best-performing ones. Almost similar behavior has been observed in the thermal distribution among selected PV module samples during thermal inspections. The temperature difference between them, in terms of inhomogeneity and thermal distribution, has been approximately 10 °C, without any hot spots being detected. As consequence, the dominant failure, with its optical effects, has led to reductions in I_{sc} and P_{max}, with the impact being especially pronounced in the worst-performing PV module due to the high severity of this failure compared to the best-performing sample. Furthermore, the V_{oc} has been more affected in the worst-performing PV module compared to the best-performing PV sample, likely due to increased thermal distribution inhomogeneity in the former. As a consequence, the ongoing impact on both affected parameters, I_{sc} and V_{oc}, has been contributing to a continuous reduction in maximum power output (P_{max}). Regarding internal resistance, the R_{oc} has exhibited slightly high values in both selected PV samples, with the best-performing sample showing a marginally higher rate. This increase in R_{oc} is attributed to corrosion failure, with the difference in R_{oc} values corresponding to variations in the severity of corrosion between the samples. In contrast, the R_{sh} exhibits differing values between the two PV samples, primarily due to the inhomogeneous distribution of observed failures. The increase in R_{sh} values is related to the rising severity of this distribution. Hence, the FF exhibits a relatively high value, attributed to the low R_{oc} and R_{sh} values, which result from the low severity of corrosion-related failures and low thermal inhomogeneity. The temperature coefficient in terms of $TC_{V_{oc}}$ has been exhibiting a consistently lower rate in the best-performing PV sample compared to the worst-performing module, with a noticeable variation between them. This trend suggests that $TC_{V_{oc}}$ has been behaving similarly to V_{oc} and R_{sh}, influenced by similar factors. The $TC_{P_{max}}$ has been showing a decreasing trend, with a notably larger reduction in the worst-performing PV sample compared to the best-performing one. This behavior suggests that degradation and failure severity have had a consistent impact on $TC_{P_{max}}$, where its behavior closely aligns with that of P_{max}, as reflected in the observed electrical performance. Nevertheless, it is important to note that this work considers only the temperature coefficients provided in the datasheet ($TC_{I_{sc}}$, $TC_{V_{oc}}$, and $TC_{P_{max}}$). The potential relationship between the observed failures and other temperature coefficients, such as $TC_{I_{mpp}}$, $TC_{V_{mpp}}$, and TC_{FF}, has not been explored in this work.

3.2.4. Type D

Type D PV modules exhibit a single dominant failure: PV cell fragmentation, while discoloration is present with very low severity. This dominate failure is notably more severe in the worst-performing sample compared to the best one, both in occurrence and in the affected area. A similar trend is observed in thermal distribution, with increased inhomogeneity related to the dominant failure. For electrical parameters, the slight increase in failures severity and the resulting thermal variation have an effect on I_{sc}, and V_{oc}, respectively, which, in turn, impacts P_{max}. In which, both selected PV modules demonstrate nearly identical electrical performance, particularly for I_{sc} and P_{max}, with the primary difference observed in V_{oc}. This suggests that the dominant failure mainly affects V_{oc} due to its inhomogeneity distribution. Although the increased severity of the exhibited failures impacts I_{sc}, and P_{max}, but even though, their performance is still higher than expected. Nevertheless, in terms of internal resistance, R_{oc} increases due to PV cell fragmentation, which results in broken interconnections (cell fingers), with this effect more pronounced in the worst-performing sample, causing a higher R_{oc} value. In contrast, R_{sh} displays low value with slight variation between these PV samples, attributed to relatively low inhomgenity thermal. Accordingly, the FF exhibits a low value, primarily due to reduced internal resistances, which are influenced by the low severity of the associated failures and their low thermal distribution. Examining temperature coefficients, $TC_{V_{oc}}$ exhibits a low rate and low variation between the best- and worst-performing modules, aligning with the low thermal inhomogeneity and suggesting that $TC_{V_{oc}}$ is related to V_{oc} and R_{sh}, both influenced by thermal effects. Conversely, $TC_{P_{max}}$ shows a slight initial low rate with low variation between PV samples, likely corresponding with P_{max} changes driven by degradation and failures in the modules.

3.2.5. Type E

The Type E PV module primarily suffers from snail trail (Microcracks) failure, identified as the dominant failure mode in both selected PV samples. Increased severity of this failure is evident in the worst-performing sample, as indicated by a higher occurrence and length of cracks (snail trails) on PV cells, ultimately leading to broken interconnections in the cell fingers. The varying distribution and severity of this failure between the two PV samples result in distinct thermal behaviors, with the worst-performing module exhibiting higher thermal inhomogeneity and more severe hotspots compared to the better-performing sample. Electrical inspection shows that the increased failure severity, including hotspot occurrence, significantly impacts V_{oc}, while I_{sc} remains less affected, resulting in a noticeable reduction in P_{max}. Furthermore, severe PV cell cracking caused by this failure leads to broken interconnections, causing a substantial increase in R_{oc}, while the inhomogeneous failure distribution influences R_{sh}. Hence, the FF shows a difference between the best- and worst-performing modules, primarily due to the important increase in both internal resistances caused by the severity of PV cell cracking and the presence of hot spots. Regarding temperature coefficients, two distinct behaviors have been observed for this module type. In the better-performing module, PV cell cracking and micro-cracking result in noticeable effects on both temperature coefficients: $TC_{V_{oc}}$ increases, while $TC_{P_{max}}$ decreases. In contrast, the worst-performing module, with severe cracking and high failure inhomogeneity, experiences extensive hotspots, significantly impacting the temperature coefficients with an increase in both $TC_{V_{oc}}$ and $TC_{P_{max}}$.

4. Correlation summary

Degradation is a complex mechanism, as highlighted earlier in this work. One of the primary factors contributing to this complexity is the simultaneous occurrence of multiple failures with varying severity levels and thermal distributions, each affecting temperature coefficients, electrical parameters, and internal resistance differently. In this context, this section presents a summary of the key findings obtained in this work, as outlined in Table 3, with a brief description provided below. Note, the (+) mark and its number indicate the extent to which the corresponding table cells are affected.

- Temperature coefficients: The temperature coefficients ($TC_{V_{oc}}$, $TC_{P_{max}}$) exhibit different behaviors. $TC_{V_{oc}}$ is primarily related to thermal homogeneity distribution, whereas $TC_{P_{max}}$ is affected by the exhibited failures and their thermal distribution. This is because $TC_{P_{max}}$ is more influenced by these factors along with others such as $TC_{I_{mpp}}$, $TC_{V_{mpp}}$, and TC_{FF}. Nevertheless, in this work, only the temperature coefficients ($TC_{I_{sc}}$, $TC_{V_{oc}}$, and $TC_{P_{max}}$) given in the datasheet have been considered.
- Electrical PV parameters: The current I_{sc} is primarily affected by optical failures or defects that reduce electrical current flow, such as PV cell cracking. In contrast, the V_{oc} is influenced by increased thermal inhomogeneity caused by specific failure-induced thermal distributions. As consequence, the P_{max} is reduced due to its dependence on both voltage and current, making it susceptible to various failure mechanisms, including failure severity and thermal distribution.
- Internal resistance: The resistance R_{oc} is associated with failures that impact the electrical connections within the PV module, particularly non-optical failures such as broken finger interconnections, corrosion, and PV cell cracking, as referred in this work. On the other hand, the R_{sh} is primarily affected by the thermal inhomogeneity distribution of the failures within the PV module, regardless of the specific type of failure. Besides, these variations in internal resistance significantly influence the FF, with increases in R_{oc} and decreases in R_{sh} both contributing to a reduction in fill factor.
- Increased severity and thermal distribution: The increasing severity of failures has significantly affected PV parameters, primarily the $TC_{P_{max}}$, while also influencing I_{sc} and R_{oc}, depending on whether the failure is optic or not. These effects have ultimately contributed to the reduction of P_{max}. Furthermore, the increased thermal inhomogeneity distribution caused by failures has affected parameters such as $TC_{V_{oc}}$, and R_{sh}, leading to a direct or indirect decline in P_{max}.
- The observed variations in temperature coefficients particularly $TC_{V_{oc}}$ and $TC_{P_{max}}$ can be attributed to the severity and thermal distribution of the occurring failures. Specifically, deviations in $TC_{V_{oc}}$ are strongly associated with the extent of thermal inhomogeneity, regardless of the failure type. In contrast, deviations in $TC_{P_{max}}$ reflect the combined effects of both the severity of the failures whether optic or non optic and their corresponding thermal distribution.

5. Summary of findings, conclusions, future work, and recommendations

This paper analyzes and provides insights into various temperature coefficients, primarily those listed in the datasheets of five different PV module types. By selecting the best- and worst-performing PV samples, this work investigates the potential correlations between temperature coefficients and failure occurrence, considering both optic and non-optic degradation mechanisms. Furthermore, it examines their relationship with other diagnostic assessments, including visual and thermal failure inspections, characteristic curve and electrical parameter evaluations, internal resistance measurements, and derived performance ratios. The key findings are summarized as follows:

$TC_{I_{sc}}$ has not been considered in this study due to its high dependence on irradiance variations, which lead to significant errors in its determination. Nevertheless, the findings suggest that $TC_{I_{sc}}$ may be influenced by optic failures and could be related to I_{sc} as an electrical parameter and R_{oc} in terms of internal resistance. However, further investigations are required to confirm this hypothesis.

$TC_{P_{max}}$ has been affected by all observed failures, regardless of their type (optic or non-optic), along with the resulting thermal inhomogeneity distribution. Furthermore, $TC_{P_{max}}$ has shown a correlation with $TC_{V_{oc}}$, as evidenced in this work. However, it is also expected to be related to other temperature coefficients ($TC_{I_{sc}}$, $TC_{I_{mpp}}$, $TC_{V_{mpp}}$, and TC_{FF}), a suggestion that requires further investigation. Furthermore, $TC_{P_{max}}$ has been primarily correlated with P_{max} as an electrical parameter and is also linked to V_{oc}, both internal resistances (R_{oc} and R_{sh}), and fill factor (FF). Therefore, all these influencing factors and correlations ultimately contribute to a direct or indirect impact on $TC_{P_{max}}$.

The increasing severity and distribution of observed failures amplify their impact on temperature coefficients, electrical parameters, and internal resistance depending on the failure type. Besides, variations in $TC_{V_{oc}}$ are closely associated with thermal inhomogeneity, while $TC_{P_{max}}$ reflects the combined severity of both physical failures and thermal distribution. These deviations serve as valuable indicators for detecting underlying failures and assessing thermal distribution within the PV modules.

As future work, this work will be extended to include the other temperature coefficients ($TC_{I_{mpp}}$, $TC_{V_{mpp}}$, and TC_{FF}) while also focusing on improving the accuracy of $TC_{I_{sc}}$ determination under outdoor conditions.

Recommendation: One key outcome of this study is the recommendation that PV module manufacturers include additional temperature coefficient values ($TC_{I_{mpp}}$, $TC_{V_{mpp}}$, and TC_{FF}) on the module nameplate or datasheet. These coefficients hold significant importance for assessing and comparing PV module performance, providing a more comprehensive understanding of their behavior under varying operating conditions.

Table 3
Summary of the correlation between PV failures, temperature coefficients, electrical parameters, and internal resistances.

Failure Nature	Failures Type	Affected PV Types	Severity	Thermal homogeneity	Temperature coefficients		Electrical parameters			Internal resistances	
					$TC_{V_{oc}}$	$TC_{P_{max}}$	I_{sc}	V_{oc}	P_{max}	R_{oc}	R_{sh}
Optic failures	Discoloration	A,C, D	Low	Yes		+	+		+		
			high	Yes		++	++		++		
			Low	No	+	++	+	+	++		+
	Delamination	B,C	Low	Yes		+	+		+		
			high	Yes		++	++		++		
			Low	No	+	++	+	+	++		+
Non-optical failures	Broken finger interconnections	A,D,E	Low	Yes		+			+	+	
			high	Yes		++			++	++	
			Low	No	+	++		+	++	+	+
	Corrosion	B	Low	Yes		+			+	+	
			high	Yes		++			++	++	
			Low	No	+	++		+	++	+	+
	PV cells fragments	D,A, E	Low	Yes		+	+		+	+	
			high	Yes		++	++		++	++	
			Low	No	+	++	+	+	++	+	+
	Snail trail along with Hot-spot	E,D, A	Low	Yes	+	+	+	+	++	+	+
			high	Yes	++	++	++	++	+++	++	++
			Low	No	+++	+++	+	++	+++	+	+++

Finally, this work calls on scientific committees and researchers to collaborate in advancing the analysis of PV module temperature coefficients, emphasizing their behavior and correlation with various failure types, severities, and distributions, as well as their integration with other PV inspection techniques. Considering the influence of diverse climatic conditions, operational environments, exposure durations, and PV module technologies is crucial. This collective effort could pave the way for a more comprehensive and alternative approach to enhancing failure detection and performance evaluation.

CRediT authorship contribution statement

N. Belhaouas: Writing – review & editing, Writing – original draft, Validation, Resources, Project administration, Methodology, Investigation, Conceptualization. **H. Hafdaoui:** Data curation, Formal analysis, Investigation, Methodology. **J.M. Nunzi:** Formal analysis, Investigation, Methodology, Writing – original draft, Writing – review & editing. **S. Khatir:** Conceptualization, Formal analysis, Validation, Writing – original draft, Writing – review & editing. **D. Ernst:** Conceptualization, Validation, Writing – original draft, Writing – review & editing. **F. Mehareb:** Conceptualization, Data curation, Formal analysis, Investigation, Resources, Software. **N. Madjoudj:** Formal analysis, Methodology, Resources, Visualization. **H. Assem:** Formal analysis, Investigation, Writing – original draft, Writing – review & editing. **D. Saheb-Koussa:** Resources, Validation, Writing – original draft, Writing – review & editing.

Declaration of competing interest

The authors declare that they have no known competing financial interests or personal relationships that could have appeared to influence the work reported in this paper.

Data availability

Data will be made available on request.

References

[1] Y. Ghorbani, S.E. Zhang, G.T. Nwaila, J.E. Bourdeau, D.H. Rose, Embracing a diverse approach to a globally inclusive green energy transition: Moving beyond decarbonisation and recognising realistic carbon reduction strategies, J Clean Prod 434 (2024) 140414.

[2] Y. Shang, S. Sang, A.K. Tiwari, S. Khan, X. Zhao, Impacts of renewable energy on climate risk: A global perspective for energy transition in a climate adaptation framework, Appl. Energy 362 (2024) 122994.

[3] M. Chaib, A. Benatiallah, A. Dahbi, N. Hachemi, F. Baira, A. Boublia, B. Ernst, M. Alam, Y. Benguerba, Long-term performance analysis of a large-scale photovoltaic plant in extreme desert conditions, Renew. Energy 236 (2024) 121426.

[4] S.D. Agyeman, B. Lin, Nonrenewable and renewable energy substitution, and low carbon energy transition: Evidence from north african countries, Renew Energ 194 (2022) 378–395.

[5] M.F. Bashir, U.K. Pata, L. Shahzad, Linking climate change, energy transition and renewable energy investments to combat energy security risks: Evidence from top energy consuming economies, Energy 314 (2025) 134175.

[6] E. Iakovou, E.N. Pistikopoulos, J. Walzberg, F. Iseri, H. Iseri, N.J. Chrisandina, S. Vedant, C. Nkoutche, Next-generation reverse logistics networks of photovoltaic recycling: Perspectives and challenges, Sol. Energy 271 (2024) 112329.

[7] J. Montes-Romero, N. Heinzle, A. Livera, S. Theocharides, G. Makrides, J. Sutterlueti, S. Ransome, G.E. Georghiou, Novel data-driven health-state architecture for photovoltaic system failure diagnosis, Sol Energy 279 (2024) 112820.

[8] W. Liu, B. Xu, Y. Liu, S. Li, W. Yan, A field-function methodology predicting the service lifetime of photovoltaic modules, Renew Sustain. Energy Rev 192 (2024) 114266.

[9] M. Mehdi, N. Ammari, A. Alami Merrouni, S. Elhamaoui, M. Dahmani, Innovative design and field performance evaluation of a desert-adapted pv module for enhanced solar energy harvesting and reliability in harsh arid environments, Appl. Energy 366 (2024) 123359.

[10] D. Hassan Daher, L. Gaillard, C. Menezo, Experimental assessment of long-term performance degradation for a pv power plant operating in a desert maritime climate, Renew. Energy 187 (2022) 44–55.

[11] H. Abdulla, A. Sleptchenko, A. Nayfeh, Photovoltaic systems operation and maintenance: A review and future directions, Renew Sustain. Energy Rev 195 (2024) 114342.

[12] Almas S. Sundaram, U. Dwivedi, Predictive analysis of power degradation rate in solar pv systems emphasizing hot spots and visual effects-based failure modes, Renew. Energy 228 (2024) 120684.

[13] L. Koester, S. Lindig, A. Louwen, A. Astigarraga, G. Manzolini, D. Moser, Review of photovoltaic module degradation, field inspection techniques and techno-economic assessment, Renew Sustain. Energy Rev 165 (2022) 112616.

[14] H. Dirawi, Q. Wang, M. Hu, Y. Su, S. Riffat, A hydronic closed-loop photovoltaic cooling system designed for hot and arid regions: Performance evaluation and degradation rate/lifetime analysis, Appl. Energy 373 (2024) 123999.

[15] S. Li, W. Liu, B. Zhang, Z. Yao, Y. Zhou, Z. Guo, W. Yan, Y. Zhou, Proposing to optimize the price and warranty of photovoltaic modules on the basis of field reliability and application, J. Clean Prod 492 (2025) 144858.

[16] Q. Meng, H. Shen, J. Zheng, X. Li, Laboratory experimental analysis of crystalline silicon photovoltaic module degradation after operating over 6 years: A case study in ghana, Sol. Energy 290 (2025) 113379.

[17] L. Lillo-Sanchez, G. Lopez-Lara, J. Vera-Medina, E. Perez-Aparicio, I. Lillo-Bravo, Degradation analysis of photovoltaic modules after operating for 22 years. a case study with comparisons, Sol. Energy 222 (2021) 84–94.
[18] M. Waqar Akram, G. Li, Y. Jin, X. Chen, Failures of photovoltaic modules and their detection: A review, Appl. Energy 313 (2022) 118822.
[19] W. Tang, Q. Yang, Z. Dai, W. Yan, Module defect detection and diagnosis for intelligent maintenance of solar photovoltaic plants: Techniques, systems and perspectives, Energy 297 (2024) 131222.
[20] E. Ramadan, N.M. Moawad, B.A. Abouzalm, A.A. Sakr, W.F. Abouzaid, G.M. El-Banby, An innovative transformer neural network for fault detection and classification for photovoltaic modules, Energy Convers. Manage. 314 (2024) 118718.
[21] N. Bansal, P. Pany, G. Singh, Visual degradation and performance evaluation of utility scale solar photovoltaic power plant in hot and dry climate in western india, Case Stud. Therm. Eng. 26 (2021) 101010.
[22] N. Bansal, S.P. Jaiswal, G. Singh, Prolonged degradation and reliability assessment of installed modules operational for 10 years in 5 mw pv plant in hot semi-arid climate, Energy Sustain. Dev 68 (2022) 373–389.
[23] F. Li, D.J. Colvin, V.S. Pavan Buddha, K.O. Davis, G. Tamizhmani, Electroluminescence and infrared imaging of fielded photovoltaic modules: A complementary analysis of series resistance-related defects, Sol. Energy 276 (2024) 112704.
[24] M. Nieto-Morone, F. Rosillo, M. Munoz-Garcia, M. Alonso-Garcia, Enhancing photovoltaic module sustainability: Defect analysis on partially repaired modules from spanish pv plants, J Clean Prod 461 (2024) 142575.
[25] A.A. Hasan, A. Mahmood Zuhdi, A.M. Al-Ghaili, A.Q. Al-Shetwi, M.A. Islam, K. Prajindra Sankar, S.S. Gunasekaran, A review on silicon photovoltaic module degradations and recent identification techniques, Sol. Energy 288 (2025) 113288.
[26] F.G. Rosillo, M.B. Nieto-Morone, R. Russell, J.M. Munoz, J.R. Sanchez, J.Y. Gonzalez, M. del Carmen Alonso-Garcia, Advances in the location and repairing of ribbon interruptions in photovoltaic modules, Renew. Energy 246 (2025) 122828.
[27] W. Luo, C.E. Clement, Y.S. Khoo, Y. Wang, A.M. Khaing, T. Reindl, A. Kumar, M. Pravettoni, Photovoltaic module failures after 10 years of operation in the tropics, Renew. Energy 177 (2021) 327–335.
[28] N. Bansal, S.P. Jaiswal, G. Singh, Comparative investigation of performance evaluation, degradation causes, impact and corrective measures for ground mount and rooftop solar pv plants - a review, Sustain. Energy Technol Assessments 47 (2021) 101526.
[29] A. Ameur, A. Berrada, A. Bouaichi, K. Loudiyi, Long-term performance and degradation analysis of different pv modules under temperate climate, Renew. Energy 188 (2022) 37–51.
[30] A. Moehlecke, I. Zanesco, J.V. Zanatta Britto, M. Ly, G.E. Decian, L.T.C.P. da Silva, J.M.R. Sganzerla, B.I. da Silva Roux Leite, T.C. Policarpi, Degradation analysis of photovoltaic modules with solar cells manufactured with sio2 tio2 thin films, Renew. Energy 244 (2025) 122749.
[31] H. Yousif, Z. Al-Milaji, Fault detection from pv images using hybrid deep learning model, Sol. Energy 267 (2024) 112207.
[32] N. Belhaouas, F. Mehareb, H. Assem, E. Kouadri-Boudjelthia, S. Bensalem, F. Hadjrioua, A. Aissaoui, K. Bakria, A new approach of pv system structure to enhance performance of pv generator under partial shading effect, J. Clean. Prod. 317 (2021) 128349.
[33] N. Belhaouas, M.-S.A. Cheikh, P. Agathoklis, M.-R. Oularbi, B. Amrouche, K. Sedraoui, N. Djilali, Pv array power output maximization under partial shading using new shifted pv array arrangements, Appl. Energy 187 (2017) 326–337.
[34] X. Moreno-Vassart, F.J. Toledo, V. Herranz, V. Galiano, Relationships between remarkable points in photovoltaic i-v curves, Renew. Energy 237 (2024) 121661.
[35] E. Ozturk, E. Ogliari, M. Sakwa, A. Dolara, N. Blasuttigh, A.M. Pavan, Photovoltaic modules fault detection, power output, and parameter estimation: A deep learning approach based on electroluminescence images, Energy Convers. Manage. 319 (2024) 118866.
[36] F. Perin Gasparin, F. Detzel Kipper, F. Schuck de Oliveira, A. Krenzinger, Assessment on the variation of temperature coefficients of photovoltaic modules with solar irradiance, Sol. Energy 244 (2022) 126–133.
[37] S.A. Rahaman, T. Urmee, D.A. Parlevliet, Investigate the impact of environmental and operating conditions of infrared (ir) imaging on infrared thermography of pv modules to identify defects, Sol. Energy 245 (2022) 231–253.
[38] E.H. Amalu, O.A. Fabunmi, Thermal control of crystalline silicon photovoltaic (c-si pv) module using docosane phase change material (pcm) for improved performance, Sol. Energy 234 (2022) 203–221.
[39] E. Özkalay, A. Virtuani, G. Eder, Y. Voronko, P. Bonomo, M. Caccivio, C. Ballif, G. Friesen, Correlating long-term performance and aging behaviour of building integrated pv modules, Energy Build. 316 (2024) 114252.
[40] A. Senturk, Investigation of datasheet provided temperature coefficients of photovoltaic modules under various sky profiles at the field by applying a new validation procedure, Renew. Energy 152 (2020) 644–652.
[41] H. Wang, X. Cheng, H. Yang, W. He, Z. Chen, L. Xu, D. Song, Potential-induced degradation: Recombination behavior, temperature coefficients and mismatch losses in crystalline silicon photovoltaic power plant, Sol. Energy 188 (2019) 258–264.
[42] B.R. Paudyal, A.G. Imenes, Investigation of temperature coefficients of pv modules through field measured data, Sol. Energy 224 (2021) 425–439.
[43] N. Belhaouas, F. Mehareb, E. Kouadri-Boudjelthia, H. Assem, S. Bensalem, F. Hadjrioua, A. Aissaoui, H. Hafdaoui, A. Chahtou, K. Bakria, D. Saheb-Koussa, The performance of solar pv modules with two glass types after 11 years of outdoor exposure under the mediterranean climatic conditions, Sustain. Energy Technol Assess 49 (2022) 101771.
[44] N. Belhaouas, H. Hafdaoui, F. Hadjrioua, H. Assem, N. Madjoudj, A. Chahtou, F. Mehareb, Failures and performance of different aged pv modules operated under northern algerian climate conditions: Analysis, assessment, and recommended solutions, Eng Fail. Anal 163 (2024) 108504.
[45] A. Osama, G.M. Tina, A. Gagliano, G. Jimenez-Castillo, F.J. Munoz-Rodriguez, Effect of electrical operating conditions on thermal behavior of pv modules: Numerical and experimental analysis, Sol. Energy Mater. Sol. Cells 287 (2025) 113625.
[46] M. Piliougine, A. Oukaja, M. Sidrach-de Cardona, G. Spagnuolo, Temperature coefficients of degraded crystalline silicon photovoltaic modules at outdoor conditions, Prog Photovolt: Res Appl 29 (2021) 558–570.
[47] G. Makrides, B. Zinsser, G.E. Georghiou, M. Schubert, J.H. Werner, Temperature behaviour of different photovoltaic systems installed in cyprus and germany, Sol. Energy Mater. Sol. Cells 93 (2009) 1095–1099.
[48] B. Li, C.W. Hansen, X. Chen, D. Diallo, A. Migan-Dubois, C. Delpha, A. Jain, A robust i–v curve correction procedure for degraded photovoltaic modules, Renew. Energy 224 (2024) 120108.
[49] F. Wardi, M. Louzazni, M. Hanine, E. Baghaz, S. Padmanaban, Optimizing photovoltaic parameters with monte carlo and parallel resistance adjustment, Energy Convers. Manage. 25 (2025) 100833.